JTTEE5 8:559-564

Impact of High Velocity Cold Spray Particles

R.C. Dykhuizen, M.F. Smith, D.L. Gilmore, R.A. Neiser, X. Jiang, and S. Sampath

(Submitted 20 November 1998; in revised form 12 May 1999)

This article presents experimental data and a computational model of the cold spray solid particle impact process. Copper particles impacting onto a polished stainless steel substrate were examined in this study. The high velocity impact causes significant plastic deformation of both the particle and the substrate, but no melting was observed. The plastic deformation exposes clean surfaces that, under the high impact pressures, result in significant bond strengths between the particle and substrate. Experimental measurements of the splat and crater sizes compare well with the numerical calculations. It was shown that the crater depth is significant and increases with impact velocity. However, the splat diameter is much less sensitive to the impact velocity. It was also shown that the geometric lengths of the splat and crater scale linearly with the diameter of the impacting particle. The results presented will allow a better understanding of the bonding process during cold spray.

Keywords coating, cold spray, computational, experimental

1. Introduction

Cold spray processing (or simply cold spray) is a high-rate material deposition process in which small, unmelted powder particles (typically 1 to 50 μm in diameter) are accelerated to velocities on the order of 500 m/s and greater by a supersonic gas jet. Upon impact with a target surface, the solid particles and the substrate deform greatly. Successive impacts result in a continuous coating of the substrate with good bond strength (Ref 1). Cold spray was developed in the mid 1980s at the Institute of Theoretical and Applied Mechanics of the Siberian Division of the Russian Academy of Science in Novosibirsk (Ref 2, 3). A recent article examined analytically the acceleration of the particles by the supersonic nozzle (Ref 4). The article also described the cold spray processing equipment and summarized the advantages of the cold spray process over other spray coating processes. Gilmore et al. (Ref 5) presented experimental data for velocity and deposition efficiency of cold spray particles and compared data to an analytical model.

The actual mechanism by which the solid state particles deform and bond has not been well characterized. It seems plausible, though it has not yet been demonstrated, that plastic deformation may disrupt thin surface films, such as oxides, and provide intimate conformal contact under high local pressure, thus permitting bonding to occur. This hypothesis is consistent with the fact that a wide range of ductile materials, such as metals and polymers, have been cold spray deposited. Experiments with nonductile materials, such as ceramics, have not been successful unless they are codeposited along with a ductile matrix material. This hypothesis would also explain the observed minimum critical velocity necessary to achieve deposition because sufficient kinetic energy must be available to plastically deform the solid material to break up surface oxides.

This article provides experimental measurements of particle splats and impact craters. Numerical model simulations of the impact process are also presented. The two methods show reasonable agreement. By combining experimental results and numerical modeling, the disadvantages of each method are minimized. The experimental technique does not allow an exact description of each impact event. The impact velocity that corresponds to each individual crater is not available. However, a particle velocity distribution was obtained from each experimental condition. The exact size, shape, and orientation of the individual impacting particles was also unknown. However, the volume of the impacting particle was determined from the total volume of the resulting splat. Use of a numerical model provides definition of each impacting event and allows variation of any parameter to obtain trends. However, the numerical model is limited by any inaccuracy that may exist in the constitutive model that describes the high strain rate impact event.

R.C. Dykhuizen, M.F. Smith, D.L. Gilmore, and **R.A. Neiser,** Sandia National Laboratories, Albuquerque, NM 87185-0835; and **X. Jiang** and **S. Sampath,** Center for Thermal Spray Research, Department of Materials Science and Engineering, State University of New York at Stony Brook, Stony Brook, NY 11794-2275. Contact e-mail: rcdykhu@sandia.gov.

2. Experimental Details

2.1 Procedures and Materials

The Sandia National Laboratories cold spray facility was used to produce copper particle impacts onto a polished 304 stainless steel substrate. Powder was fed axially into a converging-diverging nozzle 25 mm upstream of the 2 mm diameter throat. The exit aperture of the nozzle was rectangular: 2 mm wide by 10 mm long. The distance between the throat and exit aperture was 80 mm, and the nozzle expanded linearly in one dimension. The nozzle was oriented normal to the substrate. Helium was used as the accelerating gas, with inlet pressures and temperatures up to 3.4 MPa (500 psig) and 500 °C. Further details of the experimental setup are provided by Gilmore et al. (Ref 5).

The standard operation was only modified to greatly decrease the powder flux to enable examination of individual impacts. This was achieved by turning off the powder carrier gas just prior to passing the gun over the substrate. Due to the downward orientation of the nozzle and powder feed tube, it

was possible to obtain a repeatable tapering off of the powder flow. Because of the low powder gas flow during normal operation (on the order of 10% of the main gas flow), it was thought that this change did not significantly alter the powder impact velocities during the experiments from those observed during standard operation. This was confirmed by comparison with numerical predictions of the powder velocity using a previously published gas dynamic model of the system (Ref 4).

Figure 1 shows the gas-atomized powder used in these experiments (ACuPowder 500A; Union, New Jersey). The figure demonstrates that the powder was reasonably spherical. The powder diameter was measured by a Coulter laser diffraction system and found to have a mean of 22 μm with a standard deviation of 5.6 μm. Metallography of particle cross sections (not shown) indicated that the powder was near full density.

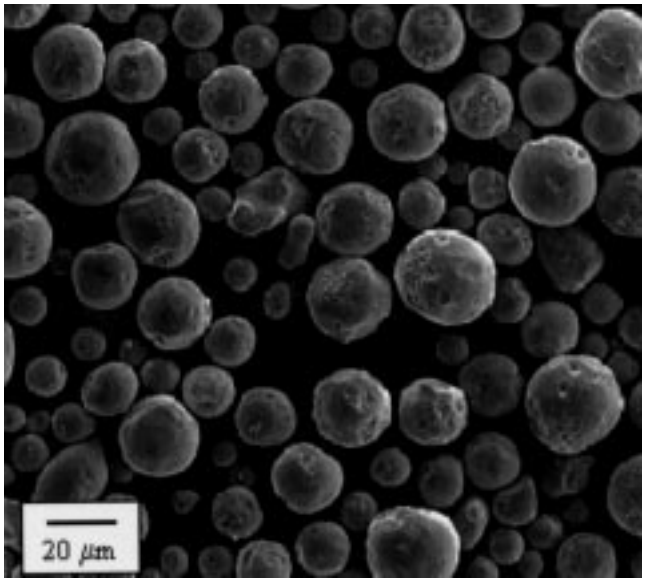

Fig. 1 A 22 μm copper powder used in the cold spray experiments

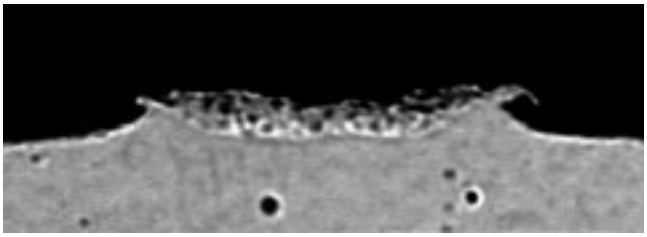

Fig. 2 Cross section of a splat created by the impact of a 700 m/s copper particle onto a stainless steel substrate. Note the stainless steel that has been ejected from the crater, which appears on the lower surface of the splat edge.

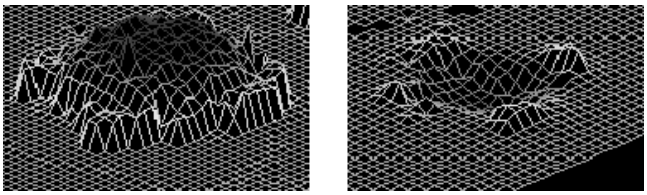

Fig. 3 Profilometry results for a splat and its crater from a 600 m/s impact

The cold spray system parameters were varied to yield mean particle impact velocities from 400 to 700 m/s per second in increments of 100 m/s. The actual mean velocities were 403, 521, 606, and 704 m/s. The standard deviation in the velocity was measured to be about 10% of the mean for all experimental conditions. From here on the nominal mean velocities will be used in this article.

2.2 Splat Measurements

The particle impact splats were examined by cross sectioning the splat after deposition. Figure 2 shows a typical result for a 700 m/s impact. Note the crater created in the stainless steel substrate. Also note that some of the steel ejected from the crater appears on the downward facing surface near the splat edge. The distance from edge to edge of the splat in this figure is 25 μm. However, it was not possible to determine if the cross section intersects the center of the splat. This makes determination of the particle size difficult.

Therefore, an alternate procedure was used to examine the splats produced. The deposited splats were examined using a scanning white light interferometer (Ref 6) to determine the shape of the top surface. Because of the system limitations, overhangs resulted in a vertical profile because the laser light cannot examine underneath an overhang.

After the initial profilometry, the copper splats were dissolved by nitric acid. Careful weighing of substrates before and after exposure to the acid revealed that the substrate was not attacked by the etchant. By repositioning the profilometer above the previously examined locations, the craters that existed underneath each of the splats were then measured. This, when combined with the profilometry data obtained prior to etching, provided quantitative information about the splat volumes. It is likely that the small thicknesses of stainless steel that formed on the underside of overhangs (Fig. 2) were not preserved.

Figure 3 shows the output of the profilometer before and after the removal of a copper splat for a 600 m/s per second impact. It is seen that a significant crater was formed in the stainless steel substrate. Also, note that the crater formed is not axisymmetric. This may be due to the anisotropic nature of the impact that results from a projectile size that is smaller than the grain size of the stainless steel, which was found to be between 30 and 65 μm. Finally, the near vertical sides resolved by the profilometer may be indicative of the same overhang depicted in Fig. 2.

Estimates can be obtained for the volumes of various regions from the profilometer measurements. The volume of material above a reference plane (the mean undeformed surface) was measured from the before image. The volume of substrate material above and the volume of the crater below the reference surface was measured from the after image. Because of conservation of substrate volume during plastic deformation, these latter two numbers correlated well. However, experimental measurement errors and difficulty in setting a precise reference surface level resulted in some disagreement.

By a simple subtraction of the before and after heights, and integration over the splat surface, the volume of the impacting copper particle was determined. Or equivalently, the volume of the particle can be determined from a combination of the volumes determined above and below the reference surfaces. From the particle volume, an equivalent preimpact diameter of each

copper particle was estimated, assuming fully dense spheres before impact.

It should be noted that the measured deposition efficiencies of copper onto stainless steel vary from essentially 0% for the 400 m/s condition to 98% for the 700 m/s condition. In fact, it was not possible to find 70 splats to measure on the 400 m/s substrate (as was done for the other conditions). The 400 m/s data set consists of only 26 splats. There were many empty craters found in the substrate for this condition, which indicated impacts of particles with velocities below the minimum required for bonding.

It is likely that the profilometry data for the 400 m/s is skewed toward the higher velocity particles in the distribution. That is, because the smaller than average particles will achieve a higher than average velocity, it is these particles that will bond to the substrate and be counted by the process, which was, indeed, observed. Figure 4 shows the equivalent preimpact particle diameter of the recovered splats as a function of the impacting velocity. It is seen that the mean particle diameter for the 400 m/s experiment is significantly lower than those measured for the other experimental conditions.

As can be seen from Fig. 4, for the 500, 600, and 700 m/s experiments, the equivalent preimpact particle diameter was reasonably approximated by the 22 μm mean obtained by a laser diffraction measurement of the original powder particles. In the data reduction process, there was a significant effort to sample the entire range of splat sizes. With this criterion in mind, it was difficult to maintain the proper proportion of each splat size so that the exact means of the size distributions could be reproduced. However, it was still intended that the mean of each sampled subset would be representative of the process.

3. Experimental Observations

Many of the experimental observations are presented as trends with the nominal mean particle impact velocity. However, it should be noted that the individual splats are created during a single experimental run from a variety of particle sizes. These particles each had velocities that were distributed around the mean. Typically, the smaller particles will travel faster (Ref 7).

It was found that the crater depth was a strong function of the impact velocity. Figure 5 shows this function where the subsurface crater volume is normalized by the volume of the copper particle that caused the crater. This plot shows that the normalized crater volume increases significantly with the impact velocity. Again, the graph presents mean values for the data sets obtained at each velocity. The standard deviation for the normalized crater volume was approximately 50% of the mean. This large amount of scatter was potentially due to experimental error in the profilometer measurements and integration of the profilometer data, various nonspherical geometries, variations in angle of impact, and variations in the actual impact velocity (scatter around the mean).

The second data curve presented in Fig. 5 helps determine which of the previously mentioned factors contributes the most to the scatter in the normalized crater volume. The mean of the ratio of the splat diameter to the equivalent particle diameter as a function of the nominal mean impact velocity is displayed. This ratio is often called a flattening ratio. It is seen that the flattening ratio is relatively insensitive to the impact velocity. The standard deviation of the flattening ratio is only 10% of the mean. The fact that the nondimensional crater volume data used to generate Fig. 5 has a 50% standard deviation, versus only a 10% standard deviation for the flattening ratio data, is due to the variations in the impact velocity within each experiment. Because the flattening ratio is insensitive to the impact velocity, variations of the impact velocity will not result in variations of the flattening ratio. However, the normalized crater volume is sensitive to the impact velocity. Therefore, the known variations of the impact velocities, also shown in Fig. 5, can reasonably account for the observed variations in the crater volume.

The scatter in the experimental data was greatly reduced by scaling the measurements with the volume (or diameter) of the individual impacting particle. Figure 6 illustrates this procedure, which shows a plot of the actual (nonscaled) particle volume and the actual crater volume for the 500 m/s data set. The large amount of scatter in both quantities is apparent. However, this plot also clearly shows the correlation between these two

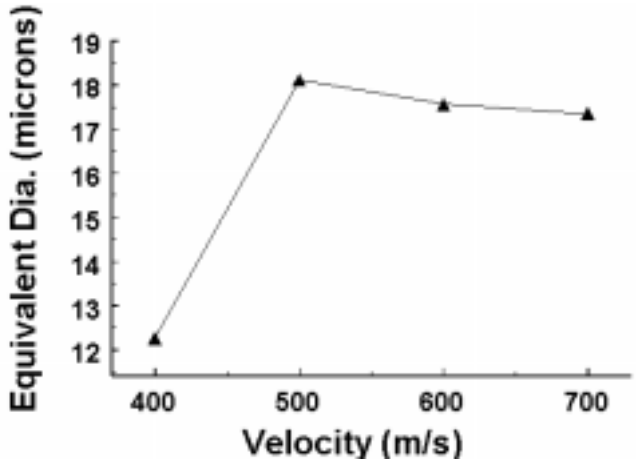

Fig. 4 Mean equivalent preimpact particle diameter (calculated from experimentally measured splat volume) as a function of nominal mean particle velocity

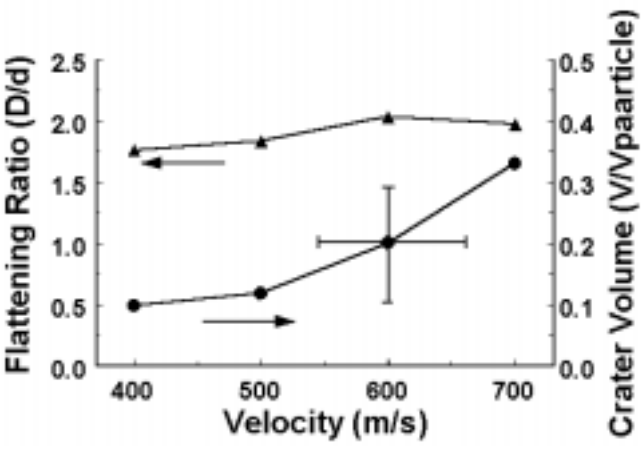

Fig. 5 Experimentally measured mean splat ratio and mean crater volume as functions of impact velocity. The crater volume is normalized by scaling with the corresponding particle volume. The error bars show the standard deviation of experimental data at the 600 m/s nominal condition.

quantities. The ratio of the largest to smallest particle volumes obtained from the data in Fig. 6 is a factor of 43. This is equivalent to a factor of 3.5 in the particle diameter, which is roughly equal to the ratio of largest to smallest particle diameters from the examination of the original powder. This provides additional confidence in the data collection process. Errors in determining the original particle diameter are due to profilometry measurement errors, interpolation of the profilometry during the integration process, and porosity of the powder, which would disappear during the impact. Thus, perfect agreement between the particle sizes obtained from the two methods is not expected.

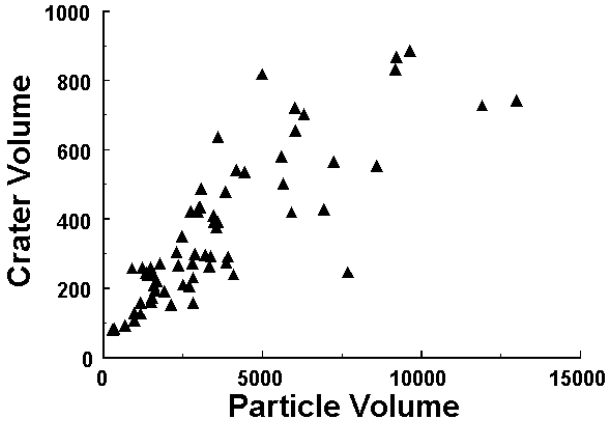

Fig. 6 Actual crater volume plotted against particle volume (both in cubic microns) from the 500 m/s data set

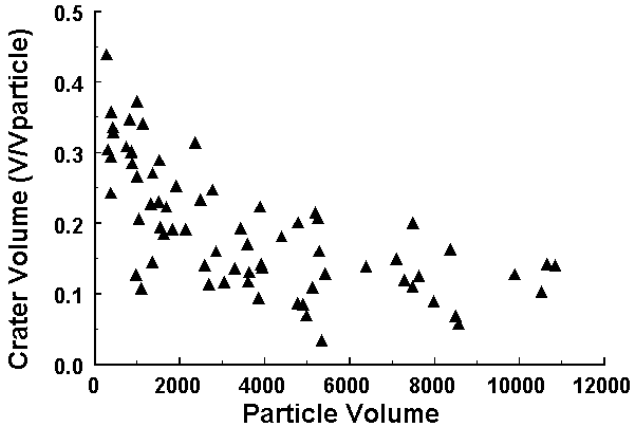

Fig. 7 Nondimensional crater volume plotted against volume of particle (in cubic microns) from the 600 m/s data set

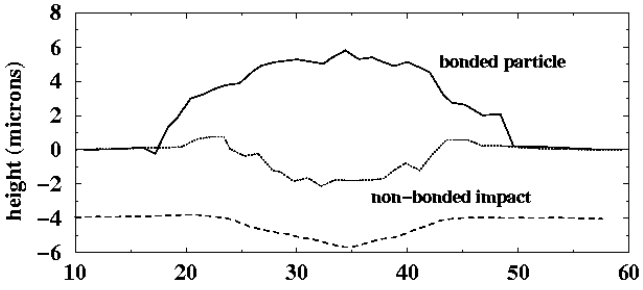

Fig. 8 Comparison of impact geometries for a bonded particle (above) and a nonbonded impact (below). Coordinates are in microns.

Figure 7 shows the normalized crater volume plotted against the particle volume for the 600 m/s data set. This reveals that there is a tendency for smaller particles to have a greater portion of their volume below the substrate surface. This is further indication that the smaller particles travel faster when exposed to the same gas conditions. It should be noted that the normalized crater volume plotted in Fig. 7 shows the opposite trend from the actual volume plotted in Fig. 6. The explanation of the apparent discrepancy is that a larger particle makes a larger crater; however, a larger particle travels more slowly and results in a smaller normalized crater, as seen in Fig. 5.

4. Bonding Mechanism

The bonding mechanism is of great interest. It has been proposed that large deformations and pressures are required to achieve intimate contact of clean metal surfaces. In this method the bonding process is very similar to the explosive welding process (Ref 8, 9). It is generally accepted that the formation of a solid-state jet of metal at the impact point of two metal plates promotes good bonding in explosive welding. Thus, the geometry and impact velocities are adjusted to assure that this jet forms at the moving contact point. This jet is credited with breaking up any surface layers and causing better contact of the two metal plates. Examination of the craters created in the cold spray process reveals evidence of jet formation. Figure 2 shows that both stainless steel and copper can be ejected from the crater. Figure 8 compares the craters created from an impact event where bonding has occurred and an impact event where it did not. Both craters depicted came from the same substrate, which was exposed to impacts that averaged near 500 m/s. However, it is likely that the empty crater is the result of a slower than average impact. The measured deposition efficiency was 9% for this experimental condition, and the standard deviation in the velocity was 60 m/s. In general, crater lips appear sharper in the craters where the particle has bonded; whereas, empty craters appear smoother. Because of the profilometry process, overhangs, as shown in Fig. 2, are not seen. It is proposed that the sharper lip is an indication of large deformations that may result in exposure of clean fresh surfaces for bonding.

5. Numerical Results

A numerical model was set up to investigate the impact process. This model enabled trend examination in the impact process with various changes in the input that were not possible experimentally. For example, the experiments could only determine a probability density function for the impact velocity of each crater, so much of the experimental scatter was due to a distribution in the velocity of the particles that created the various craters at each system setting. With a numerical model, it is easy to specify the impact velocity exactly.

The Sandia National Laboratories generated computer code CTH (Ref 10) was developed to model a wide range of solid dynamics problems involving shock wave propagation and material motion in one, two, or three dimensions. The code uses a two-step Eulerian solution scheme. The first step is a Lagrangian step in which the cells distort to follow the material

motion. The second step is a remesh step, where the distorted cells are mapped back to the original Eulerian mesh. The mesh size used is 0.2 μm in both radial and axial directions. This mesh size was required to enable solutions that were not mesh size dependent.

The simulations presented in this paper are normal angle impacts of fully dense spherical particles. This allowed the assumption of an axisymmetric, two-dimensional geometry. The CTH code includes various models for material properties. These material models predict the viscoplastic response of various materials (principally metals) based on a consideration of thermally activated dislocation mechanics. The assumed forms take into account the effects of isotropic strain hardening, thermal softening, strain rate dependency, and pressure-dependent shear and yield strengths. All of the available material models were investigated, each of which gave slightly different splat shapes. However, they all gave the same general trends, as reported in this article.

In the results presented in this article, the Steinberg-Guinan-Lund viscoplastic model (Ref 11, 12) was used to model the stainless steel substrate. Rate-dependent parameters were not available for this material. However, this model has been successfully used in other impact studies at Sandia National Laboratories for stainless steel targets. The Zerilli-Armstrong model (Ref 13) was used for the copper particles. This model includes history and rate-dependent parameters to describe the mechanical response of the copper.

The substrate modeled was 200 μm in diameter. Figure 9 shows the final splat shape in cross section obtained from a CTH run using a 25 μm particle impacting at various velocities onto a stainless steel substrate. Detailed examination of the numerical output reveals that a peak temperature of 1200 K was obtained for the 700 m/s impact (which is below the copper melting temperature of 1360 K). In fact, CTH overestimates material temperatures because dissipation via conduction is not modeled. When these calculations are rerun with a 20 μm particle, the geometric results are all scaled proportionally, which agrees with the experimental observations.

The 400 m/s impact results in the lowest impact pressure and lowest deformations as expected. It was experimentally found that this condition does not result in bonding of the particle to the substrate. Note that there is no indication of any jet formation from the 400 m/s impact, but a jetlike ejection of both stainless steel and copper from the crater was shown at the higher velocities. It was proposed that this jetlike flow aids in bonding by a similar mechanism for bonds created in explosive welding conditions. In the CTH simulations, all impacts were assumed to result in bonding unless a fracture stress value is predicted.

Comparing the experimental result in Fig. 2 to the 700 m/s impact shown in Fig. 9 reveals both similarities and differences. They both also show a gradual decrease in the substrate height away from the impact site. They both show a lip angled away from the splat. However, Fig. 2 shows that the lip is composed mostly of copper, and the numerical result shows the opposite. The penetration of the splat is overpredicted by the numerical simulation. This may be due to improper modeling of the large strain rates or incorrect material properties. The copper may be stronger than modeled due to the small grain size associated with the rapid cooling during powder formation. The stainless steel grain size is comparable to the splat size, which results in anisotropic behavior. In fact, the craters formed in the laboratory experiments were typically not axisymmetric (see Fig. 3).

Figure 10 shows the flattening ratio and the crater depth calculated as functions of impact velocity. These agree reasonably well with the experimental measurements shown in Fig. 5. The flattening ratio was determined by using the distance from the crater center to the tip of the crater lip as the splat radius. The experimental trends were reproduced, that is, the flattening ratio was largely independent of the impact velocity, and the crater depth increased monotonically with impact velocity.

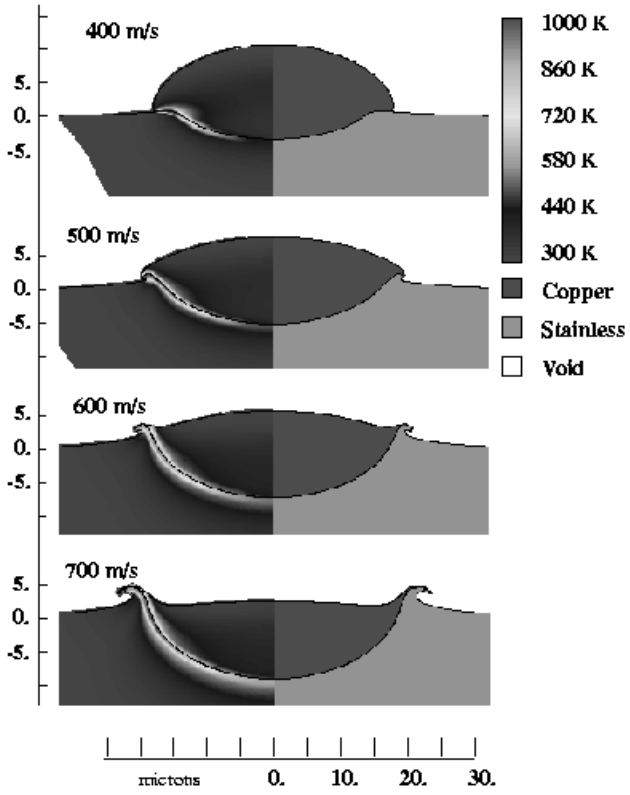

Fig. 9 Diameter splat shapes, 25 μm, calculated by CTH. The left side shows temperature; the right side shows material type. The original substrate surface is at 0 μm on the left-hand scale.

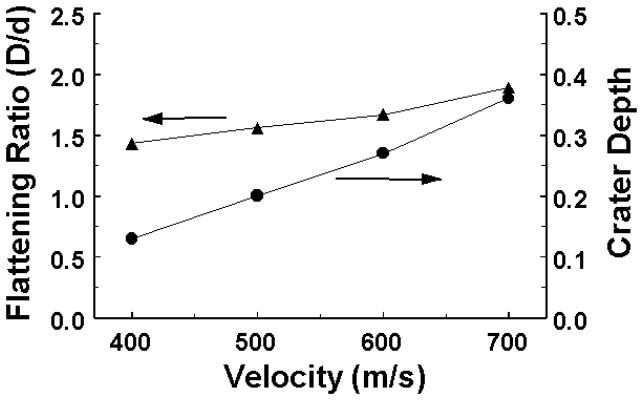

Fig. 10 Calculated flattening ratio and crater depth as functions of velocity. Crater depth is normalized by the particle diameter.

The pressure generated by the impact as a function of position and time can be obtained from the computer simulations. These are, of course, less than the maximum impact pressure, as derived by Lord Rayleigh, for a one-dimensional impact onto a nonyielding substrate (Ref 14):

$$P_{max} = \rho C v \quad \text{(Eq 1)}$$

The peak pressure magnitude obtained from the numerical simulations was approximately one-third of the product given in Eq 1. The reduction is due to the multidimensional impact and the yielding substrate.

The pressure at the central impact point was found to reach this peak in a time period that can be approximated by the particle diameter divided by the impact velocity (approximately 50 ns). It was these large pressures (on the order of 5 GPa), combined with the large deformations of the particle and substrate, that exposed clean surfaces and resulted in bonding. The CTH code assumes that all contacting surfaces result in an intimate bond between the layers; so unfortunately, this code cannot be used to determine the critical velocity for bonding.

6. Conclusions

By both numerical and experimental methods, it has been demonstrated that cold spray deposition of copper onto stainless steel substrates results in significant cratering of the substrate. Greater impact velocity results in deeper craters. It was also shown that the radius of the resultant splats was insensitive to the impact velocity, except for velocities too small to be of interest in cold spray processes. Geometric sizes of the splat and crater were found to scale with the initial particle diameter. It is proposed that the large deformations caused by the solid state jetting of both substrate and particle materials from the crater promoted bonding of the particle to the substrate. Neither the particle nor the substrate need to be melted to obtain high bond strengths.

Acknowledgments

The authors would like to thank E.S. Hertel for his patient assistance in use of the CTH code and K.H. Eckelmeyer and A. Kilgo for metallographic analysis. Sandia National Laboratories is a multiprogram laboratory operated by Sandia Corporation, a Lockheed Martin Company, for the United States Department of Energy under contract DE-AC04-94AL85000. The work at SUNY was supported in part by the MRSEC program of the National Science Foundation under award 96-32570.

References

1. R.C. McCune, A.N. Papyrin, J.N. Hall, W.L. Riggs, and P.H. Zajchowski, An Exploration of the Cold Gas-Dynamic Spray Method for Several Materials Systems, *Thermal Spray Science and Technology*, C.C. Berndt and S. Sampath, Ed., ASM International, 1995, p 1-5
2. A.P. Alkhimov, A.N. Papyrin, V.F. Kosarev, N.I. Nesterovich, and M.M. Shushpanov, Gas Dynamic Spraying Method for Applying a Coating, Patent 5,302,414, April 12, 1994
3. A.O. Tokarev, Structure of Aluminum Powder Coatings Prepared by Cold Gas Dynamic Spraying, *Met. Sci. Heat Treat.*, Vol 38 (No. 3-4), 1996, p 136-139
4. R.C. Dykhuizen and M.F. Smith, Gas Dynamic Principles of Spray, *J. Therm. Spray Technol.*, Vol 7 (No. 2), 1998, p 205-212
5. D.L. Gilmore, R.C. Dykhuizen, R.A. Neiser, T.J. Roemer, and M.F. Smith, Particle Velocity and Deposition Efficiency in the Cold Spray Process, *J. Therm. Spray Technol.*, Vol 8 (No. 4), 1999, p 576-582
6. P.J. De Groot and L. Deck, Surface Profiling by Analysis of White-Light Interferograms in the Spatial Frequency Domain, *J. Modern Optics*, Vol 42 (No. 2), 1995, p 389-401
7. R.A. Neiser, J.E. Brockman, T.J. Ohern, M.F. Smith, R.C. Dykhuizen, T.J. Roemer, and R.E. Teets, Wire Melting and Droplet Atomization in a High Velocity Oxy-Fuel Jet, *Thermal Spray Science and Technology*, C.C. Berndt and S. Sampath, Ed., ASM International, 1995, p 99-104
8. B. Crossland, *Explosive Welding of Metals and Its Application*, Claredon Press, Oxford, 1982
9. H. El-Sobky, Mechanics of Explosive Welding, *Explosive Welding, Forming and Compaction*, T.Z. Blazynski, Ed., Applied Science Publishers, London, 1983
10. E.S. Hertel, R.L. Bell, M.G. Elrick, A.V. Farnsworth, G.I. Kerley, J.M. McGlaun, S.V. Petney, S.A. Silling, and L. Yarrington, *Lance CTH: A Software Family for Multi-Dimensional Shock Physics Analysis*, *Shock Waves at Marseille*, Vol 1, R. Brun and L.Z. Dumitrescu, Ed., Springer-Verlag, 1995, p 377-382
11. D.J. Steinberg, S.G. Cochran, and M.W. Guinan, A Constitutive Model for Metals Applicable at High Strain Rate, *J. Appl. Phys.*, Vol 51, 1980, p 1498
12. D.J. Steinberg and C.M. Lund, A Constitutive Model for Strain Rates from 10-4 to 106 sec-1, *J. Appl. Phys.*, Vol 65, 1989, p 1528
13. F.J. Zerilli and R.W. Armstrong, Dislocation Mechanics-Based Constitutive Relations for Material Dynamics Calculations, *J. Appl. Phys.*, Vol 61, 1987, p 1816
14. D.S. Drumheller, *Introduction to Wave Propagation in Nonlinear Fluids and Solids*, Cambridge University Press, 1998